Bull. Mater. Sci., Vol. 37, No. 4, June 2014, pp. 789–796. © Indian Academy of Sciences.

Rapid hydrothermal route to synthesize cubic-phase gadolinium oxide nanorods

SAMIRAN HAZARIKA, NIBEDITA PAUL and DAMBARUDHAR MOHANTA*

Department of Physics, Tezpur University, Tezpur 784 028, India

MS received 21 July 2013; revised 12 September 2013

Abstract. **An inexpensive fabrication route and growth mechanism is being reported for obtaining quality gadolinium oxide (Gd_2O_3) nanoscale rods. The elongated nanoscale systems, as produced via a hydrothermal process, were characterized by X-ray diffraction (XRD), high resolution transmission electron microscopy (HRTEM), optical absorption spectroscopy, photoluminescence (PL) spectroscopy, Raman spectroscopy and magnetic hysteresis measurements. XRD patterns of the nanorods, as-prepared from independent precursors of different pH, depict a cubic crystal phase and an average crystallite size of 5–6·5 nm. As revealed from HRTEM micrographs, diameter of the nanorods prepared at pH = 13·3 (~ 7 nm) was much smaller than the rods prepared at pH = 10·8 (~ 19 nm). However, the aspect ratio was more than double in the former case than the latter case. PL response was found to be dominated by defect mediated emissions, whereas Raman spectrum of a given specimen (pH = 10·8) has revealed characteristic $F_g + A_g$ modes of cubic phase of Gd_2O_3 nanorods, apart from other independent modes. Furthermore, $M \sim H$ plot of the nanorod system (pH = 10·8) exhibited slight departure from the ideal superparamagnetic behaviour, with low remanence and coercive field values. The exploitation of one-dimensional Gd_2O_3 nanorods have immense potential in the production of advanced contrast agents, smart drives and also in making novel ferrofluids of technological relevance.**

Keywords. **Hydrothermal; nanostructure; rare-earth; gadolinium oxide.**

1. Introduction

In recent years, compared to bulk and other low dimensional structures, elongated nanostructures such as nanowires, nanorods and nanotubes have gained remarkable research interest owing to their novel electrical, optical and magnetic properties (Du and Tendeloo 2005). Organized, but anisotropic growth of one-dimensional (1-D) systems, under specific environment, has emerged as an area of topical interest with immense potential in the field of nanophotonics, high performance nanophosphors and other functional elements (Holmes *et al* 2000; Bockrath *et al* 2001; Huang *et al* 2001; Li and Xia 2003; Xia *et al* 2003). On the other hand, rare-earth (RE) oxide based nanostructures are found to be promising candidates in the field of high throughput luminescent devices, catalysis and other functional devices based on their excellent electronic, optical and physicochemical responses arising from 4*f* electrons (Tang *et al* 2003). Not surprisingly, all these properties could be largely influenced by their chemical composition, crystal structure, shape and dimensionality (Xu *et al* 2009).

1-D nanostructures can be developed by several methods, such as chemical and physical vapour processes (Yu *et al* 2004), laser ablation (Duan and Lieber 2000), solution phase (Trentler *et al* 1995), arc discharge (Choi *et al* 2000), hydrothermal treatment (Du *et al* 2001, 2003; Dhananjaya *et al* 2012a, b), vapour-phase transport process (Wu and Yang 2000) and template-based method (Huang *et al* 2000). Above all, hydrothermal synthesis technique has a unique advantage as it is capable of providing high purity and high yield, apart from homogeneously grown anisotropic nanostructures. Besides, hydrothermal technique does not use any catalyst and template. Production of 1-D gadolinium oxides and hydroxides by hydrothermal method have been reported by many authors. Gadolinium oxide (Gd_2O_3) exists in three different crystallographic forms: hexagonal, monoclinic and cubic (Bai *et al* 2009). Owing to its thermal and chemical stabilities, narrow emission (Gai *et al* 2011) and having a wide direct bandgap of 5·3 eV (Singh *et al* 2004), Gd_2O_3 is believed to be a promising host for a number of applications. It can be an useful candidate in the deployment of waveguide devices (Guo *et al* 2004), high dielectric constant components and other such devices. On the other hand, elongated RE oxides have recently been applied to drug delivery and competitive immunoassays (Liu *et al* 2012). However, transforming bulk Gd_2O_3 powder into its hydroxide product and later to 1-D nanorods by subsequent dehydration is rarely found

*Author for correspondence (best@tezu.ernet.in)

in the literature. To be specific, obtaining elongated RE nanorods from the bulk powder, short synthesis time along with a catalyst free approach are the main features of the present work.

Herein, we demonstrate production of 1-D Gd_2O_3 nanorods via a user-friendly and cost-effective hydrothermal route, without using any sort of catalyst or template. The effect of pH was discussed in the light of growth mechanism of the nanorods. Characteristic properties with respect to structural, optical emission and magnetic responses of the synthesized nanorods are discussed.

2. Experimental

2.1 *Synthesis of Gd_2O_3 nanorod powder*

A simple hydrothermal procedure was carried out to produce quality Gd_2O_3 nanorods (Dhananjaya *et al* 2011). In a typical procedure, 0·28 g of bulk Gd_2O_3 (Otto, 99·9% purity) was first dispersed in 35 mL distilled water and dilute HNO_3 was added dropwise until a clear sol was obtained. pH was then adjusted to 9·2, 10·8 and 13·3 by adding several drops of 5 M NaOH solution under vigorous stirring. The mixture was then transferred to a teflon-lined stainless steel autoclave and subjected to oven heating at ~ 140 °C for 24 h. A white solid product of $Gd(OH)_3$ was then collected by filtering the precursor using a Whatman filter®. The product was washed several times, first with distilled water and then with ethanol, followed by oven-drying at 80 °C. Finally, the hydroxide powder was annealed at 600 °C, for 3 h so as to facilitate spontaneous decomposition of $Gd(OH)_3$ and consequently, dehydration to yield Gd_2O_3 nanopowder. The flow chart of hydrothermally synthesized Gd_2O_3 nanorods is shown in figure 1.

Acidification:
Gd_2O_3 (bulk) + $6HNO_3 \rightarrow 2Gd(NO_3)_3 + 3H_2O$,

Hydrolysis:
$Gd(NO_3)_3 + 3NaOH \rightarrow Gd(OH)_3 + 3NaNO_3$,

Dehydration:
$2Gd(OH)_3 \rightarrow Gd_2O_3$ (nanopowder) + $3H_2O$.

2.2 *Characterization techniques*

The crystallographic information was revealed by a Rigaku miniFlex X-ray diffractometer (XRD) that uses a CuKα source (λ = 1·54 Å). The diffraction angle was varied in the range of 20–60° and with a step angle of 0·05°. Transmission electron microscopy (TEM) images were recorded by a JEOL JEM 2100 machine, operating at an accelerating voltage of 200 kV. Thermogravimetric analysis (TGA) was performed on the hydroxide product $Gd(OH)_3$ of the sample (prepared at pH 10·8) using a TGA-50 Shimadzu thermogravimetric analyser. The optical absorption study was performed by a UV–Visible spectrophotometer (UV 2450, Shimadzu), while photoluminescence excitation and emission responses were assessed by a Perkin-Elmer LS 55 spectrophotometer. Finally, Raman measurements were recorded by using a Renishaw In-Via Raman spectrometer (Renishaw, Wotton-under-Edge, UK) equipped with an Ar^+ laser of λ = 514·5 nm, used as the excitation source. The spectrum was obtained with a measured resolution of 0·3 cm^{-1}. Lastly, magnetic hysteresis measurement was carried out on a particular specimen (prepared at pH = 10·8) at room temperature using a MPMS SQUID VSM (Quantum Design, USA).

3. Results and discussion

3.1 *Structural and morphological features along with growth mechanism*

XRD patterns of the as-synthesized $Gd(OH)_3$ prepared at pH = 10·8 and Gd_2O_3 nanorod-products prepared at pH = 9·2, 10·8 and 13·3 are depicted in figure 2(a). The hydroxide product exhibited hexagonal crystal structure with observable diffraction planes indexed as (1 1 1), (1 0 1), (2 0 1) and (0 0 2) (JCPDS no. 83-2037) (Thongtem *et al* 2010). After annealing at 600 °C, prominent, but apparently broadened diffraction peaks corresponding to (2 2 2), (4 0 0), (4 4 0) and (6 2 2) crystallographic planes suggest that nanocrystallites would crystallize into a cubic phase (JCPDS no. 86-2477) (Dhananjaya *et al* 2011). No peak due either to hydroxides, impurities or byproducts was detected. With symbols having their usual meanings and using the diffraction formula relevant to cubic phase: $d_{hkl} = (h^2 + k^2 + l^2/a^2)^{1/2} = \lambda/2 \sin\theta$, for a first-order diffraction, the crystal cell parameters ($a = b = c$) could be estimated. The lattice parameters of the samples synthesized at pH of 9·2, 10·8 and 13·3, were estimated to be 10·80, 10·83 and 10·79 Å, respectively. Earlier, a cubic-phase cell parameter of 10·81 Å was predicted for Gd_2O_3 system (Ningthousam *et al* 2009). The average crystallite size (d) and microstrain (η) can also be calculated from the popular Williamson–Hall (W–H) expression

$$\beta \cos\theta = 0{\cdot}9\lambda/d + 4\eta \sin\theta,$$

which represents the equation of a straight line. The average crystallite size was found to be ~ 5·19, 6·46 and 6·09 nm for pH 9·2, 10·8 and 13·3 cases, respectively along with a negative microstrain value of the order ~ 10^{-3} (table 1). A negative strain could be due to the relaxed nature of the nanocrystallites present in the nanorods.

HRTEM images of the nanorod samples, prepared at pH 10·8 and 13·3, are shown in figures 2(b) and (c). As for pH 10·8, a number of nanorods with an average diameter ~ 19 nm and length ranging from 76 to 115 nm are evident

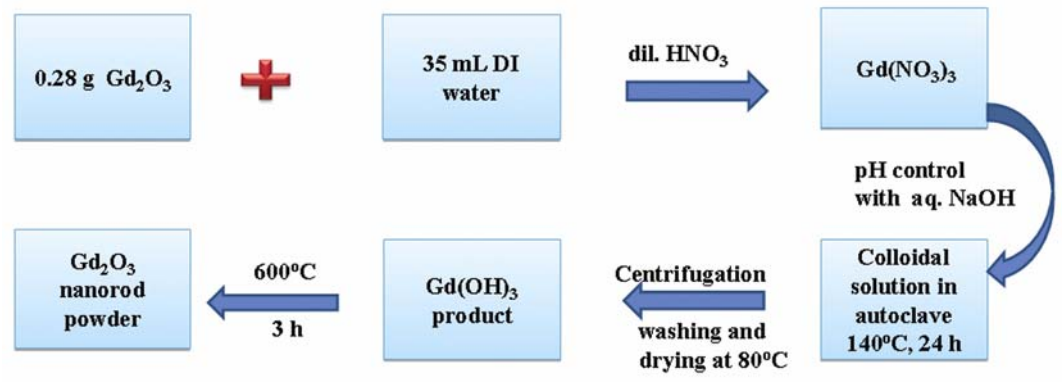

Figure 1. Block diagram of hydrothermally synthesized Gd_2O_3 nanorods.

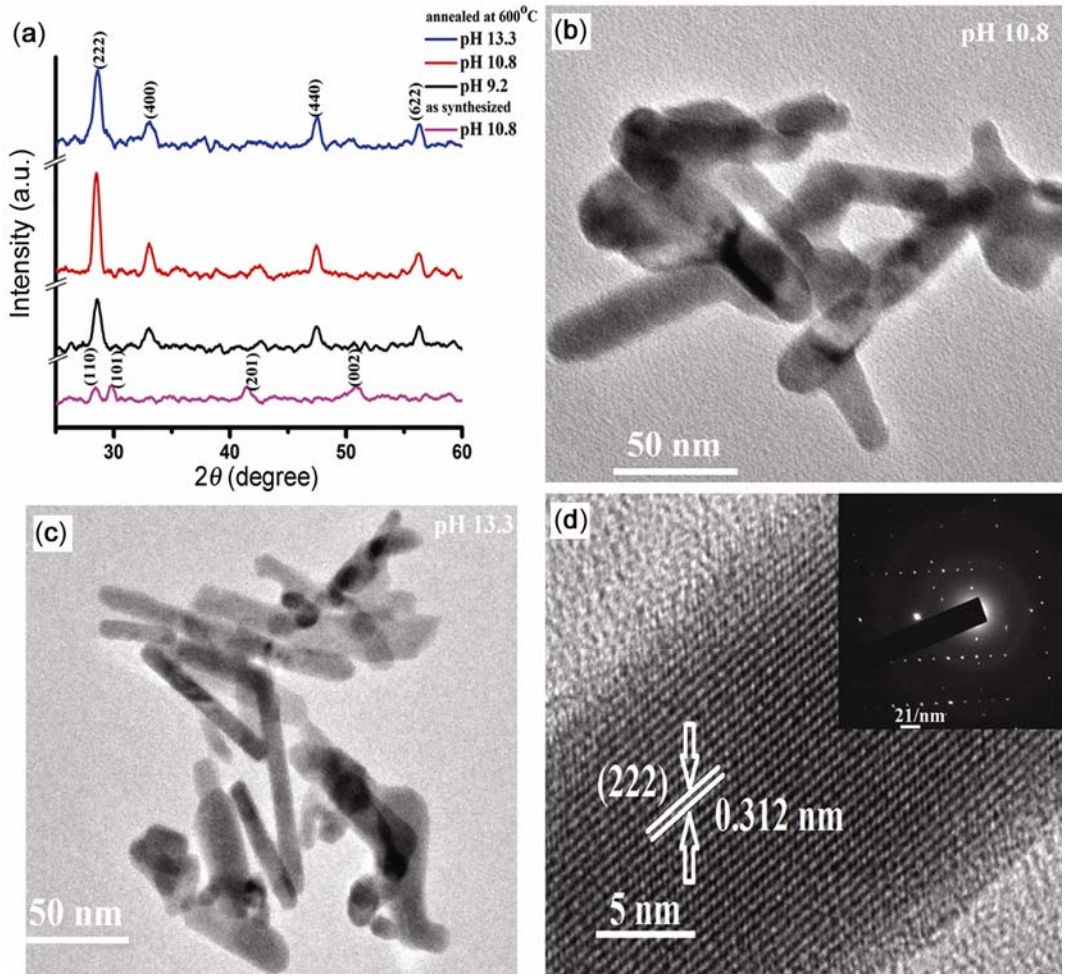

Figure 2. (**a**) XRD patterns of as-synthesized $Gd(OH)_3$ product (pH 10·8) and Gd_2O_3 nanorods derived from precursors of different pH, (**b**) and (**c**) represent HRTEM images of nanorod samples synthesized at pH 10·8 and 13·3, respectively. Magnified image of an isolated Gd_2O_3 nanorod (derived from pH 10·8 precursor) with crystal lattice fringes depicted in (**d**). The SAED pattern is being highlighted in the inset of (**d**).

in the micrograph (figure 2b). The rods resemble the structure of 'unfold fingers', with smoothened surfaces but without a branching effect. For any nanorod, the diameter at the middle of the rod was much larger than at the extreme-edge. This is ascribed to the spontaneous decomposition of gadolinium hydroxide into its oxide product followed by subsequent assimilation of crystallites along (2 2 2) plane and instant termination at the end. Also, all Gd_2O_3 nanorods were not found in the same focal plane and that is why we observed a reasonable difference in

Table 1. Average crystallite size (nm), lattice parameter (nm), microstrain and dimension of nanorods (nm) of as-synthesized Gd_2O_3 nanorod systems.

Nanorods synthesized from precursors	Avg. crystallite size (d) (nm)	Lattice parameter ($a = b = c$) (nm)	Microstrain ($\times 10^{-3}$)	Dimension of nanorods		
				Length (nm)	Diameter (nm)	Aspect ratio
pH 9·2	5·19	1·080	–12·69	–	–	–
pH 10·8	6·46	1·083	–8·93	75–115	19	~4
pH 13·3	6·09	1·079	–8·54	60–128	7	~8·5

the image contrast of many off-aligned rods. In case of sample synthesized from a precursor of pH 13·3, the range of average nanorod length was found to be wider, i.e. 60–128 nm, but having a reduced average diameter of ~7·1 nm (figure 2c). Thus, both shorter and longer rods were achievable at a higher pH. We speculate that, unrestricted preferential growth of nanocrystallites might have led to longer sized rods. But shorter nanorods could have been developed due to obstruction of one nanorod growing in the vicinity of the other or, thermodynamic instability that would keep surface energy of the overall system minimum. Consequently, the diameter of the rods can also be reduced in this case. As diameter is close to the average crystallite dimension (see XRD analysis), we expect that the aligned growth is manifested by just piling up of single crystallites along a preferred direction. Whereas, nanorods derived from a precursor of lower pH (10·8), comprise of several crystallites along a direction normal to the *c*-axis preferential growth, thereby resulting in a larger diameter (~19 nm) of the rods. Considering the lower limit of the nanorod length, the aspect ratio was estimated to be ~4 and 8·5 corresponding to pH = 10·8 and 13·3 cases, respectively. A higher pH value represents a higher concentration of OH^- ions and a higher chemical potential of the precursor solution. A higher chemical potential is necessary for the growth of higher aspect ratio 1-D nanostructures (Yang *et al* 2007). In contrary to the results of Yang *et al* (2007) here, we realized that, nanorods with a higher aspect ratio could be obtained from a high pH precursor, but along with some amount of inhomogeneity. Figure 2(d) shows an enlarged view of the selected region of a nanorod of figure 2(c). A clear lattice fringe pattern suggests that the nanorod specimen is highly crystalline one with an interplanar spacing of ~0·312 nm which corresponded to the (2 2 2) crystallographic plane of the nanosystem. This is, in fact, consistent to the XRD pattern of the nano-Gd_2O_3 specimen derived from pH = 10·8. The selected area electron diffraction (SAED) pattern of the nanorods (prepared at pH 10·8) characterizes a number of arrayed bright spots thus indicating highly crystalline nature of the specimen under study.

The growth mechanism of Gd_2O_3 nanorods can be illustrated in a block diagram, shown in figure 3. The growth of Gd_2O_3 nanorods was believed to be governed by a solution-solid phase process (Wang *et al* 2004). In the hydrothermal process, several drops of aq. NaOH were added to adjust pH of the solution. According to Xu *et al* (2009), the growth morphology is neither governed by a catalyst nor directed by any template (Xu *et al* 2009). On adding aq. NaOH, the Gd^{3+} ions tend to interact with OH^- ions formed from aq. NaOH. On adding NaOH, a gentle white solution is formed which comprised of colloidal particles. The colloids, while partially dissolved in water results in a metastable supersaturated solution under hydrothermal environment. On cooling back to room temperature, a large number of seed particles of $Gd(OH)_3$ were formed through homogeneous nucleation process. It is the seed which becomes the basis of 1-D elongated nanostructures formed as a result of coherent re-crystallization process. Accordingly, the whole supersaturated solution is recrystallized to yield highly crystalline rod-shaped structures (Xu *et al* 2009). A high temperature sintering step is needed to facilitate instant dehydration thereby resulting in the desired product of Gd_2O_3 nanorods.

Thermogravimetric analysis (TGA) was carried out to assess the progressive weight loss of $Gd(OH)_3$ within a range of temperature (27–600 °C). Typically, TGA curve in figure 4 characterizes four successive, uneven steps. The first step, observable within 27–250 °C experiences a weight loss of 2·1% and is due to the (partial) dehydration of adsorbed H_2O in $Gd(OH)_3$. The second step was in the range of 250–335 °C and having a loss of ~8·02%, whereas third step was between 335 and 440 °C and with a weight loss of ~1·8%. The second and third steps, ranging from 250 to 440 °C, collectively represent decomposition of $Gd(OH)_3$ to the intermediate product of GdOOH, prior to the complete oxide product. The transformation of intermediate GdOOH to final Gd_2O_3 product is obtained in the fourth step (440–594 °C) and with a weight loss of 1·7%. The total weight loss is ~13·62%, which is comparable to an earlier prediction (~13·03%) for complete decomposition of $Gd(OH)_3$ to form Gd_2O_3 (Xu *et al* 2009).

3.2 *Optical absorption, emission and phononic features*

UV–Visible absorption spectroscopy is the most common but an important spectroscopy tool which is capable of revealing electronic transitions of a particular valence

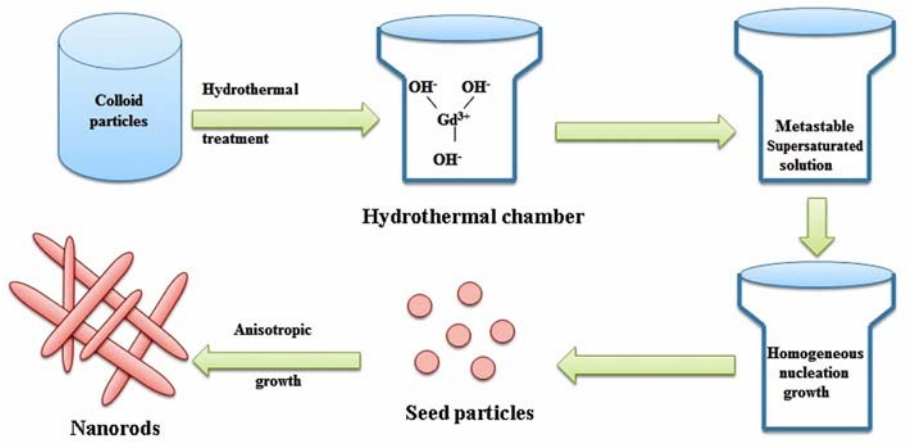

Figure 3. A scheme of growth mechanism illustrating formation of Gd_2O_3 nanorods.

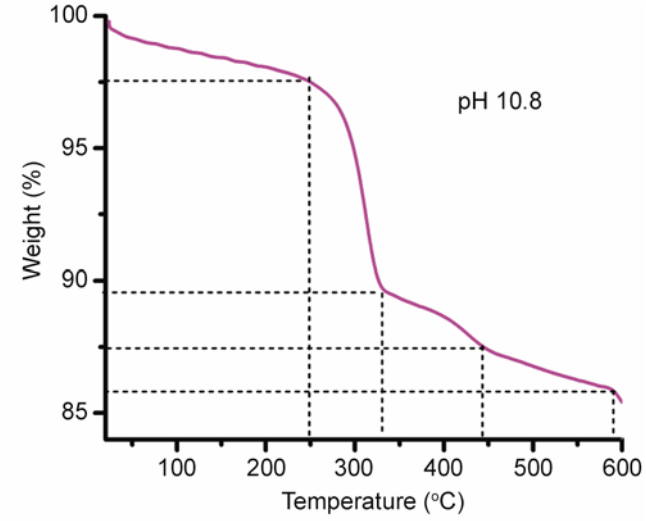

Figure 4. Thermogravimetric analysis of unsintered $Gd(OH)_3$ product (pH 10·8).

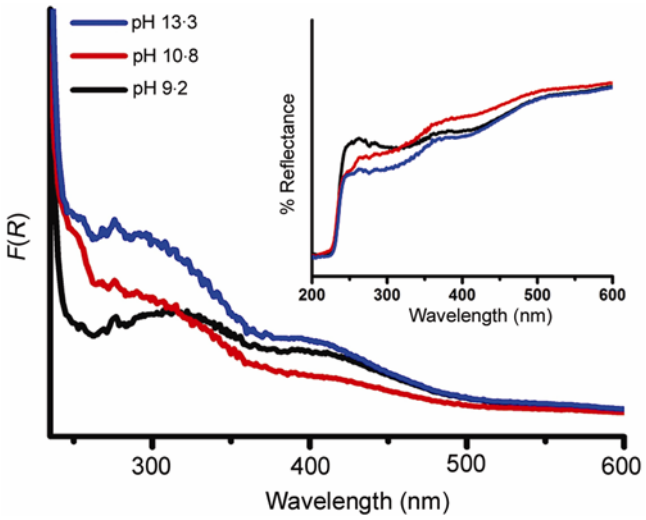

Figure 5. Kubelka–Munk plot representing $F(R)$ as absorbance (inset shows actual reflectance spectra).

state. Either absorbance or reflectance (where absorption is not strong) can be employed to determine such transitions. The absorption spectra as obtained from the reflectance data of our nanorod samples are shown in figure 5. The reflectance spectra being shown as the inset of figure 5. For conversion, we have used popular Kubelka–Munk equation

$$F(R) = (1 - R)^2/2R,$$

where R represents reflectance and $F(R)$ the corresponding absorbance (Han *et al* 2007). Gd^{3+} has [Xe] $4f^7$ configuration, which means it has half-filled shell having a $^8S_{7/2}$ ground state. The energy absorption in Gd is mediated via transition of $4f$ electrons to $5d$ level and then reorganization of $4f$ electrons into various multiplets. The seven electrons in $4f$ orbitals of Gd have as many as 3432 multiplets and the ground state is $^8S_{7/2}$ (Rahman *et al* 2011; Hazarika and Mohanta 2013). Among these multiplets, the low lying multiplet above the ground state is $^6P_{7/2}$. Essentially, two absorption peaks were observed in the spectra. The absorption peak positioned at ~274 nm is typical for Gd_2O_3 nanorods and is attributed to $^8S_{7/2} \rightarrow {}^6I_{7/2}$ transition (Rahman *et al* 2011). The peak positioned at ~398 nm, may be attributed to recombination of delocalized electrons close to the conduction band with a single charged state of surface oxygen vacancy as per Wang's proposition (Hu *et al* 2007; Zhang *et al* 2009). The peak at ~274 nm has a strong absorption feature, particularly for the nanorod specimen derived at a higher pH value.

Photoluminescence spectroscopy is a powerful technique to understand the nature of radiative transitions and defect related emission response of a material system. Figure 6(a) shows room temperature photoluminescence excitation (PLE) spectra of pH 10·8 Gd_2O_3 nanorods monitored at an emission wavelength of ~480 nm. The peaks, in PLE spectra, often represent absorption characteristics of the system under study. Basically, Gd^{3+} has a simpler absorption spectrum in comparison to the other

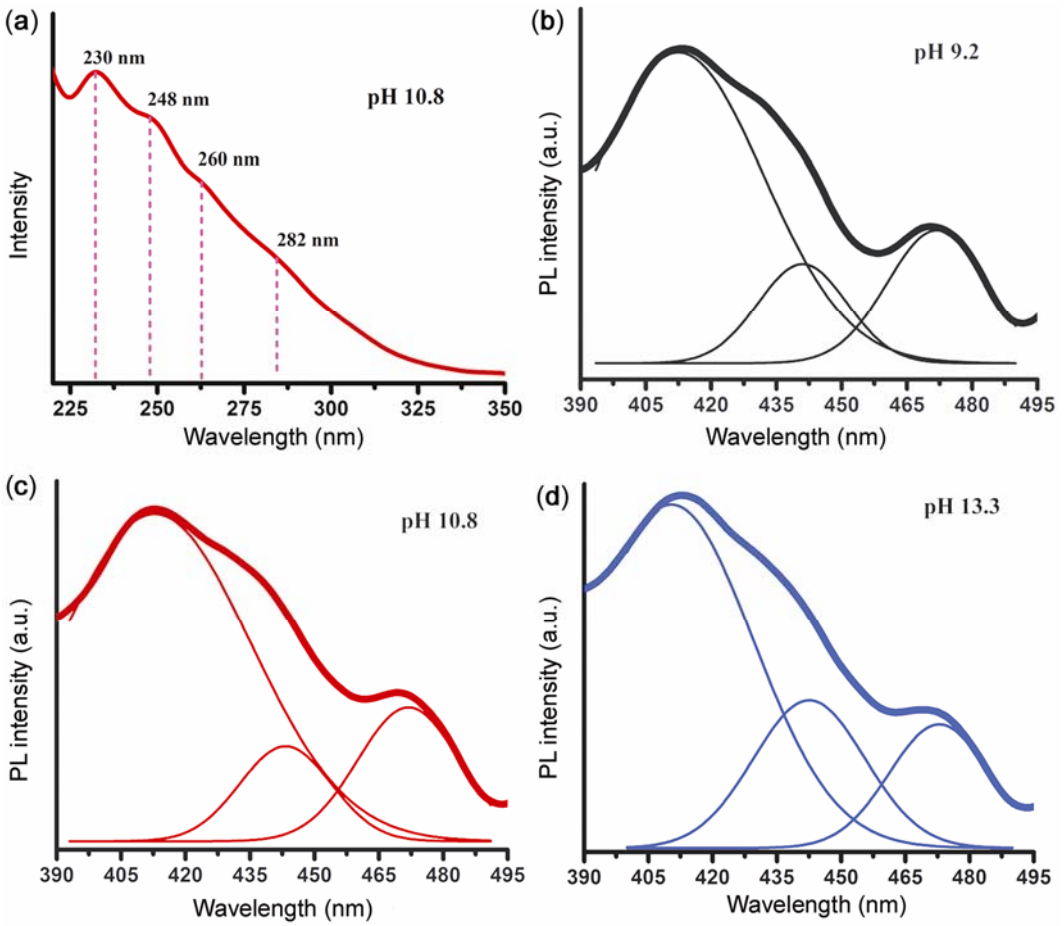

Figure 6. Room temperature (**a**) PL excitation spectrum of nanorod sample (pH 10·8) considering λ_{em} = 480 nm and PL emission spectra (with deconvolution) corresponding to λ_{ex} = 300 nm, obtained for all three samples derived at (**b**) pH 9·2, (**c**) pH 10·8 and (**d**) pH 13·3.

trivalent RE ions. Note that, the ground state energy level for Gd^{3+} is $^8S_{7/2}$ level. As can be found, the excitation spectra have clearly revealed four important peaks, positioned at ~230, 248, 260 and 282 nm. The 230 nm emission peak is attributed to the excitation band of Gd_2O_3 host (Pang *et al* 2003). The peak at ~248 nm is ascribed to one of the transitions corresponding to $^8S_{7/2} \rightarrow {}^6I_{j/2}$ multiplets, where j = 9, 12, 13, 15 and 17 (Mukherjee *et al* 2008). The band observed at ~260 nm is assigned to $^8S_{7/2} \rightarrow {}^6D_{9/2}$ transition (Kripal and Mishra 2010). The peak at ~282 nm is attributed to $^8S_{7/2} \rightarrow {}^6I_{7/2}$ transition (Mukherjee *et al* 2008). On the other hand, room temperature emission spectra of Gd_2O_3 nanorods, excited at a wavelength of ~300 nm are shown in figures 6(b–d) representing characteristic features of the nanorods synthesized at a pH of 9·2, 10·8 and 13·3, respectively. The asymmetrically broadened spectra signify the superimposition of several peaks of different origin. The deconvolution of each of the spectra through multiple Gaussian fitting could help extracting independent peaks, which are presented in figures 6(b–d). All the samples have showed three prominent peaks, at ~413, 442 and 472 nm. The band to band emission was not observable due to the improved defect related emission response. The peak maxima at ~413, 442 and 472 nm could be attributed to surface defects of different Schottky and Frenkel types (Dhananjaya *et al* 2012a, b). The normalized intensity ratio of ~413 to 472 nm peak increases with increasing pH value of the desired precursor. In oxide systems, typically oxygen vacancies and interstitials are vastly prevalent and the manifestation of such defects, contribute significantly to the modified photoluminescence response.

Raman spectroscopy is a versatile but non-destructive tool to explore vibrational, rotational and other low frequency modes in the systems under study. The micro-Raman spectrum of the nanorod sample synthesized at a pH of 10·8, is highlighted in figure 7. Apparently, three peaks were observed, which were characterized by Raman shifts located at ~314, 359 and 446 cm^{-1}. The peak at ~314 cm^{-1} is identified as the mixed modes of $F_g + E_g$ and the one at ~446 cm^{-1} as an independent F_g mode (Dilawar *et al* 2008). Most importantly, the prominent peak at ~359 cm^{-1} is assigned to $F_g + A_g$ modes, which mainly corresponds to the cubic phase of Gd_2O_3.

3.3 *Magnetic response of Gd_2O_3 nanorod system*

In order to assess magnetic behaviour of the synthesized product, Gd_2O_3 nanorod sample (prepared at a pH 10·8) was assessed by a SQUID magnetometer. It is known that, magnetic response changes with the pH value of the precursor solution. In particular, saturation magnetization value (M_s) varies with the particle dimension that depends largely on pH of the precursor. In this context, modified magnetic features due to an increased fraction of superparamagnetic particles was observed in an earlier work (Thakur *et al* 2009). Although magnetic measurements were not performed on all the samples, it is likely that, M_s value may vary with the aspect ratio of the nanorods (and thus with pH of the sol). As a means of general assessment (if the system is magnetic or not), magnetic measurement was performed on a well-characterized sample (pH = 10·8) the results of which are as discussed below.

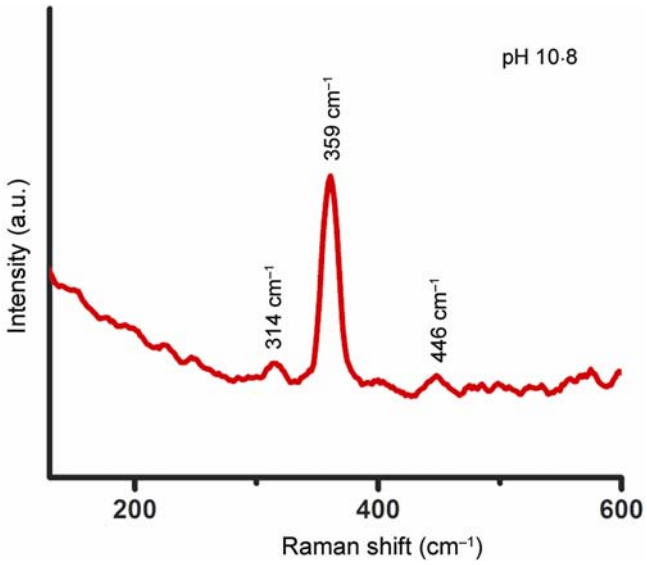

Figure 7. Raman spectrum of Gd_2O_3 nanorod sample synthesized at pH 10·8.

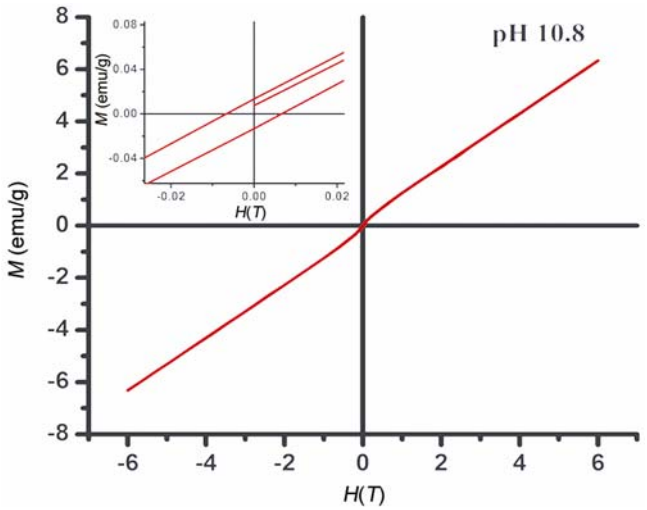

Figure 8. Room temperature $M \sim H$ plot of Gd_2O_3 nanorods synthesized at pH 10·8. Inset shows enlarged view of plot near zero-field.

Figure 8 depicts response of magnetization vs magnetic field (M–H), measured at room temperature (300 K). The magnetization feature was recorded when the applied field was varied in the range –6 to 6 T. Since no clear hysteresis was observed, we speculate that the sample is likely to be superparamagnetic. Even the saturation magnetization could not be predicted exactly. The paramagnetic nature of the nanorods containing Gd^{3+} centres is due to the presence of half-filled f orbitals with seven electrons (Mukherjee *et al* 2008). Note that characteristic paramagnetic feature of a system is caused by a number of magnetic dipole moments summing up to zero in the absence of an applied field. But the net moment becomes non-zero when the system is subjected to a field. However, superparamagnetism arises when thermal energy is strong enough to orient individual moments randomly. As far as superparamagnetism is concerned, in the past, most of the studies were devoted mostly to iron based nanostructures. We anticipate that, the paramagnetism in Gd_2O_3 nanorods has arisen from non-interacting localized nature of the magnetic moments. The magnetic properties of Gd^{3+} ions come from seven unpaired inner $4f$ electrons, which are closely bound to the nucleus and effectively shielded by the outer closed shell electrons $5s^2 5p^6$ from the crystal field. Among various paramagnetic RE ions, Gd^{3+} ions possess a high magnetic moment due to isotropic electronic ground state $^8S_{7/2}$. In order to explore further, we zoomed in $M \sim H$ response near zero field. Remarkably, M value was found to experience a non-zero value in the absence of the field ($H = 0$). This suggests that the investigated sample cannot represent an idealistic superparamagnetic system. The coercive field (H_c) and remanence (M_r) were found to be 0·0066 T and 0·0136 emu/g, respectively. A low coercive field indicates that magnetic moments can be reversed even by changing the direction of a weak applied field. In other words, order of the moments is lost at a higher magnetic field and considering a small remanence magnitude, the Gd_2O_3 nanorod sample under study behaved closely to a superparamagnetic system.

4. Conclusions

We have demonstrated production and characterization of cubic phase Gd_2O_3 nanorods, synthesized by a surfactant free hydrothermal method. XRD studies on Gd_2O_3 systems have revealed cubic phase of the as-synthesized nanorods while unsintered $Gd(OH)_3$ product showed a hexagonal phase. HRTEM analyses have revealed a remarkable distribution of nanoscale rods, with aspect

ratio nearly doubled when the precursor used was changed from pH = 10·8 to 13·3. Moreover, the evidence of a clear lattice fringe pattern of the rods and ordered bright spots as observable from SAED, suggests that the samples were highly crystalline in nature. TGA analysis on the hydroxide product has revealed the total weight loss ~ 13·62% up to a temperature of ~ 600 °C. The photoluminescence response was found to be manifested by various kinds of defects such as Schottky and Frenkel types. The prominent peak in the Raman spectra attributed to the cubic phase of the nanorods. The magnetic measurements have revealed non-ideal superparamagnetic nature of the Gd_2O_3 nanorods at room temperature.

Acknowledgements

We acknowledge UGC, New Delhi, for financial support received under major project scheme no. 37-367/2009 (SR). We would like to offer sincere thanks to the Department of Chemical Sciences, TU, for extending TGA facility. We also thank SAIF, NEHU, Shillong, for extending HRTEM facility and IIT Kharagpur, for magnetic measurements.

References

Bai L, Liu J, Li X, Jiang S, Xiao W, Li Y, Tang L, Zhang Y and Zhang D 2009 *J. Appl. Phys*. **106** 073507

Bockrath M, Liang W, Bozovic D, Hafner J H, Lieber C M, Tinkham M and Park H 2001 *Science* **291** 283

Choi Y C *et al* 2000 *Adv. Mater*. **12** 746

Duan X F and Lieber C M 2000 *Adv. Mater*. **12** 298

Du G H, Chen Q, Che R C, Yuan Z Y and Peng L M 2001 *Appl. Phys. Lett*. **79** 3702

Du G H, Chen Q, Han P D and Peng L M 2003 *Phys. Rev*. **B67** 035323

Du G and Tendeloo G V 2005 *Nanotechnology* **16** 595

Dhananjaya N, Nagabhushana H, Nagabhushana B M, Rudraswamy B, Shivakumara C, Ramesh K P and Chakradhar R P S 2011 *Physica* **B406** 1645

Dhananjaya N, Nagabhushana H, Nagabhushana B M, Rudraswamy B, Sharma S C, Sunitha D V, Shivakumara C and Chakradhar R P S 2012a *Spectrochim. Acta Part A: Mol. Biomol. Spectr*. **96** 532

Dhananjaya N, Nagabhushana H, Nagabhushana B M, Rudraswamy B, Shivakumara C and Chakradhar R P S 2012b *Bull. Mater. Sci*. **35** 519

Dilawar N, Varandani D, Mehrotra S, Poswal H K, Sharma S M and Bandyopadhyay A K 2008 *Nanotechnology* **19** 115703

Gai S, Yang P, Wang D, Li C, Niu N, He F and Li X 2011 *Cryst. Eng. Commun.* **13** 5480

Guo H, Yang X, Xiao T, Zhang W, Lou L and Mugnier J 2004 *Appl. Surf. Sci.* **230** 215

Han T Y, Wu C F and Hsieh C T 2007 *J. Vac. Sci. Technol*. **B25** 430

Holmes J D, Johnston K P, Doty R C and Korgel B A 2000 *Science* **287** 1471

Hu C G, Liu H, Dong W T, Zhang Y Y, Bao G, Lao C S and Wang Z L 2007 *Adv. Mater*. **19** 470

Huang M H, Choudrey A and Yang P 2000 *Chem. Commun*. **12** 1063

Huang Y, Duan X, Wei Q and Lieber C M 2001 *Science* **291** 630

Hazarika S and Mohanta D 2013 *Eur. Phys. J. Appl. Phys.* **62** 30401

Kripal R and Mishra I 2010 *Physica* **B405** 425

Li D and Xia Y 2003 *Nano Lett*. **3** 555

Liu Z, Liu X, Yuan Q, Dong K, Jiang L, Li Z, Ren J and Qu X 2012 *J. Mater. Chem.* **22** 14982

Mukherjee S, Dasgupta P and Jana P K 2008 *J. Phys. D: Appl. Phys*. **41** 1

Ningthoujam R S, Shukl R, Vatsa R K, Duppel V, Kienle L and Tyagi A K 2009 *J. Appl. Phys*. **105** 084304

Pang M L, Lin J, Fu J, Xing R B, Luo C X and Han Y C 2003 *Opt. Mater*. **23** 547

Rahman A T M, Vasilev K and Majewski P 2011 *J. Colloid. Interf. Sci.* **354** 592

Singh M P, Thakur C S, Shalini K, Banerjee S, Bhat N and Shivashankar S A 2004 *J. Appl. Phys.* **96** 5631

Tang Q, Liu Z, Li S, Zhang S, Liu X and Qian Y 2003 *J. Cryst. Growth* **259** 208

Thakur S, Katyal S C and Singh M 2009 *J. Magn. Magn. Mater*. **321** 1

Thongtem T, Phuruangrat A, Ham D J, Lee J S and Thongtem S 2010 *Cryst. Eng. Commun.* **12** 2962

Trentler T J, Hickman K M, Goel S C, Viano A M, Gibbons P C and Buhro W E 1995 *Science* **270** 1791

Wang G, Wang Z, Zhang Y, Fei G and Zhang L 2004 *Nanotechnology* **15** 1307

Wang Z, Quan Z and Lin J 2007 *Inorg. Chem*. **46** 5237

Wu Y and Yang P 2000 *Chem. Mater*. **12** 605

Xia Y, Yang P, Sun Y, Wu Y, Mayers B, Gates B, Yin Y, Kim F and Yan H 2003 *Adv. Mater*. **15** 353

Xu Z, Yang J, Hou Z, Li C, Zhang C, Huang S and Lin J 2009 *Mater. Res. Bull*. **44** 1850

Yu J, Yu J C, Ho W, Wu L and Wang X C 2004 *J. Am. Chem. Soc*. **126** 3422

Yang J, Li C, Cheng Z, Zhang X, Quan Z, Zhang C and Lin J 2007 *J. Phys. Chem.* **C111** 18148

Zhang N, Ran Y, Zhou L, Gao G, Shi R, Qiu G and Liu X 2009 *Mater. Chem. Phys.* **114** 160